Current Transport in Carbon Nanotube Transistors

(Invited Paper)

Mahdi Pourfath, Hans Kosina, and Siegfried Selberherr
Institute for Microelectronics, TU Wien, 1040 Vienna, Austria
Email: {pourfath|kosina|selberherr}@iue.tuwien.ac.at

***Abstract*— Carbon nanotubes (CNTs) have been studied in recent years due to their exceptional electronic, opto-electronic, and mechanical properties. To explore the physics of carbon nanotube field-effect transistors (CNT-FETs) self-consistent quantum mechanical simulations have been performed. The performance of carbon nanotube-based transistors is analyzed numerically, employing the non-equilibrium Green's function formalism. Electron-phonon interaction parameters, such as electron-phonon coupling strength and phonon energy, strongly depend on the chirality and the diameter of the carbon nanotube. The response of carbon nanotube based transistors is studied taking rigorously into account the effect of electron-phonon interaction.**

I. Introduction

Novel structures and materials such as multiple gate MOSFETs, carbon nanotube field-effect transistors (CNT-FETs), and molecular based transistors, are expected to be introduced to meet the requirements for scaling. CNTs can be considered as a graphene sheet which is wrapped into a tube. The way the graphene sheet is wrapped is described by a pair of indices (n, m) called the chiral vector. The integers n and m denote the number of unit vectors along two directions in the honeycomb crystal lattice of graphene. If $m = 0$, the CNT is called *zigzag*. If $n = m$, the CNT is called *armchair*. Otherwise, it is called *chiral*. CNTs with $n-m = 3$ are metals, otherwise they are semiconductors. Semiconducting CNTs can be used as channels for transistors [1], and metallic CNTs can serve as interconnect wires [2].

CNT-FETs have been considered in recent years as potential alternatives to CMOS devices due to their excellent electronic properties [3,4]. The most interesting properties of CNTs are quasi-ballistic carrier transport [5], suppression of short-channel effects due to one-dimensional electron transport [6, 7], and nearly symmetric structure of the conduction and valence bands, which is advantageous for complementary circuits. Moreover, owing to excellent optical properties of CNTs, an all-CNT electronic and opto-electronic circuit can be envisioned. The direct band-gap and the tunability of the band-gap with the tube diameter renders CNTs as suitable candidates for opto-electronic devices, especially for infra-red (IR) applications [8,9] due to the relatively narrow band gap.

The non-equilibrium Green's function (NEGF) method has been successfully used to investigate the characteristics of nano-scale silicon transistors [10, 11], CNT-FETs [12–14], and molecular devices [15–17]. In this work we discuss the NEGF formalism to study quantum transport in CNT-FETs.

The outline of the paper is as follows. In Section II the NEGF formalism is briefly described. The implementation of this method for CNT-FETs is presented in Section III. The electron-phonon interaction parameters of a CNT depend on the chiral vector, which implies that many different parameter values exist. In Section IV the device response is studied for some electron-phonon interaction parameters. After a brief discussion in Section V conclusions are presented in Section VI.

II. Non-equilibrium Green's Function Formalism

The NEGF formalism initiated by Schwinger, Kadanoff, and Baym allows to study the time evolution of a many-particle quantum system. Knowing the single-particle Green's functions of a given system, one may evaluate single-particle quantities such as carrier density and current. The many-particle information about the system is cast into self-energies, which are part of the equations of motion for the Green's functions. Green's functions enable a powerful technique to evaluate the properties of a many-body system, both, in thermodynamic equilibrium and non-equilibrium situations.

Four types of Green's functions are defined as the non-equilibrium statistical ensemble averages of the single particle correlation operator. The greater Green's function $G^{>}$ and the lesser Green's function $G^{<}$ deal with the statistics of carriers. The retarded Green's function G^{R} and the advanced Green's function G^{A} describe the dynamics of carriers.

$$\begin{aligned} G^{>}(1,2) &= -i\hbar^{-1}\langle\hat{\psi}(1)\hat{\psi}^{\dagger}(2)\rangle \\ G^{<}(1,2) &= +i\hbar^{-1}\langle\hat{\psi}^{\dagger}(2)\hat{\psi}(1)\rangle \\ G^{\mathrm{R}}(1,2) &= \theta(t_1-t_2)[G^{>}(1,2)-G^{<}(1,2)] \\ G^{\mathrm{A}}(1,2) &= \theta(t_2-t_1)[G^{<}(1,2)-G^{>}(1,2)] \end{aligned} \tag{1}$$

The abbreviation $1 \equiv (\mathbf{r_1}, t_1)$ is used, $\langle \ldots \rangle$ is the statistical average with respect to the density operator, $\theta(t)$ is the unit step function, $\hat{\psi}^{\dagger}(\mathbf{r_1}, t_1)$ and $\hat{\psi}(\mathbf{r_1}, t_1)$ are the field operators creating or destroying a particle at point $(\mathbf{r_1}, t_1)$ in space-time, respectively. The Green's functions are correlation functions. For example, $G^{>}$ relates the field operator $\hat{\psi}$ of the particle at point $(\mathbf{r_1}, t_1)$ in space-time to the conjugate field operator $\hat{\psi}^{\dagger}$ at another point $(\mathbf{r_2}, t_2)$.

Under steady state condition the Green's functions depend only on time differences. One usually Fourier transforms the time difference coordinate, $\tau = t_1 - t_2$, to energy. For example, the lesser Green's function is transformed as $G^{<}(1,2) \equiv G^{<}(\mathbf{r_1}, \mathbf{r_2}; E) = \int (d\tau/\hbar) e^{iE\tau/\hbar} G^{<}(\mathbf{r_1}, \mathbf{r_2}; \tau)$.

978-1-4244-2186-2/08/$25.00 ©2008 IEEE

Under steady-state condition the equation of motion for the Green's functions can be written as [18]:

$$[E - H]\, G^{\mathrm{R,A}}(1,2) - \int d3\ \Sigma^{\mathrm{R,A}}(1,3) G^{\mathrm{r,a}}(3,2) = \delta_{1,2} \tag{2}$$

$$G^{\lessgtr}(1,2) = \int d3 \int d4\ G^{\mathrm{R}}(1,3) \Sigma^{\lessgtr}(3,4) G^{\mathrm{A}}(4,2) \tag{3}$$

where H is the single-particle Hamiltonian operator, and Σ^{R}, $\Sigma^{<}$, and $\Sigma^{>}$ are the retarded, lesser, and greater self-energies, respectively.

III. Implementation

This section describes the implementation of the outlined NEGF formalism for the numerical analysis of CNT-FETs. Fig. 1 shows the structure of the simulated devices. A tight-binding Hamiltonian is used to describe the transport phenomena in CNT-FETs. The self-energy due to electron-phonon interactions are studied next.

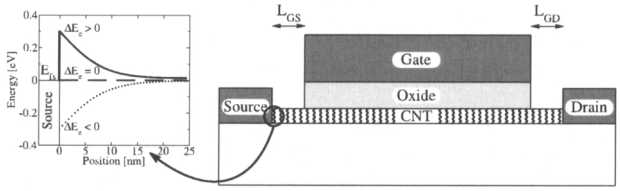

Fig. 1. Cross section of the investigated CNT based transistor and the band-edge profile at the source sided metal-CNT interface. Depending on the work function difference between metal and CNT, a positive, zero, or negative barrier height for electrons or holes can be achieved.

A. Tight-Binding Hamiltonian

In Graphene three σ bonds hybridize in an sp^2 configuration, whereas the other $2p_z$ orbital, which is perpendicular to the graphene layer, forms π covalent bonds. The π energy bands are predominantly determining the solid state properties of graphene. Similar considerations hold for CNTs. We use a nearest-neighbor tight-binding π-bond model [13]. Each atom in an sp^2-coordinated CNT has three nearest neighbors, located $a_{\mathrm{cc}} = 1.42$ Å away. The band-structure consists of π-orbitals only, with the hopping parameter $t = V_{pp\pi} \approx -2.7$ eV and zero on-site potential.

The tight-binding Hamiltonian matrix for a $(n,0)$ zigzag CNT, shown in Fig. 2-a, can be written as [13]

$$\underline{H} = \begin{pmatrix} \underline{U_1} & \underline{t_1} & & & \\ \underline{t_1} & \underline{U_2} & \underline{t_2} & & \\ & \underline{t_2}^{\dagger} & \underline{U_3} & \underline{t_1} & \\ & & \underline{t_1} & \underline{U_4} & \underline{t_2}^{\dagger} \\ & & & \underline{t_2} & \underline{U_5} \ \ . \\ & & & & \ \ . \ \ . \end{pmatrix} \tag{4}$$

where the underlined quantities denote matrices. We assume that the electrostatic potential shifts the on-site potential. Therefore, $\underline{U_i}$ is a diagonal matrix which represents the electrostatic potential energy in the ith circumferential ring of carbon atoms. Equal electrostatic potential for all carbon atoms within a ring is assumed, therefore $\underline{U_i} = U_i \underline{I}$. The first and second kind of interaction matrix between the neighboring rings are denoted by $\underline{t_1}$ and $\underline{t_2}$. Only the nearest neighbor interaction between carbon atoms is considered. The coupling matrix between Layer 2 and Layer 3 is diagonal, $\underline{t_1} = t\,\underline{I}$, where t is the hopping parameter. However, the coupling matrix between Layer 1 and Layer 2 is given by

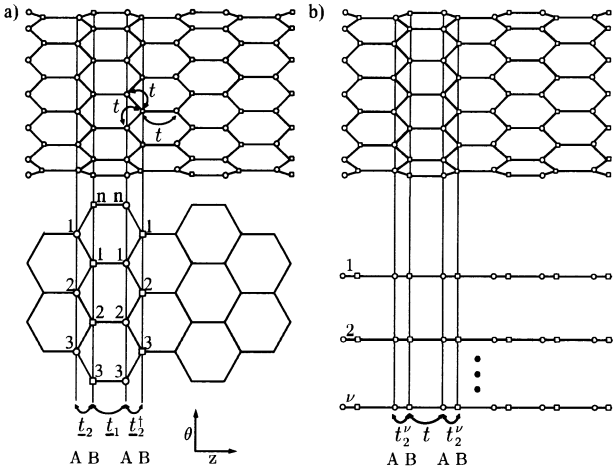

Fig. 2. Layer layout of a $(n,0)$ zigzag CNT. a) The coupling matrices between layers are denoted by $\underline{t_1}$ and $\underline{t_2}$, where $\underline{t_1}$ is a diagonal matrix and $\underline{t_2}$ includes off-diagonal elements. b) The corresponding one-dimensional chain, in mode space [11], with two sites per unit cell with hopping parameters t and $t_2^{\nu} = 2t\cos(\pi\nu/n)$.

$$\underline{t_2} = \begin{pmatrix} t & & t & \\ t & t & & \\ & t & t & \\ & & . & . \end{pmatrix} \tag{5}$$

The eigen vectors of the matrix $\underline{t_2}$ represent plane waves around the circumference of the CNT with the quantized wave-vectors $k_\nu = 2\pi\nu/\sqrt{3}a_{\mathrm{cc}}n$, where $\nu = 1, 2, \ldots n$ [13], and the eigen values $2t\cos(\pi\nu/n)$. By transforming from real space into eigen mode space [11], the subbands become decoupled and the Hamiltonian can be written as $\underline{H} = \sum_\nu \underline{H}^\nu$, where $\underline{H}^\nu$, the Hamiltonian of the subband ν, is given by

$$\mathbf{H}^\nu = \begin{pmatrix} U_1^\nu & t_1^\nu & & & & \\ t_1^\nu & U_2^\nu & t_2^\nu & & & \\ & t_2^\nu & U_3^\nu & t_1^\nu & & \\ & & t_1^\nu & U_4^\nu & t_2^\nu & \\ & & & t_2^\nu & U_5^\nu & . \\ & & & & . & . \end{pmatrix}, \tag{6}$$

where $U_i^\nu = U_i$, $t_1^\nu = t$, and $t_2^\nu = 2t\cos(\pi\nu/n)$ [13]. The one-dimensional tight-binding Hamiltonian $\underline{H}^\nu$ describes a chain with two sites per unit cell with on-site potential U_i^ν and hopping parameters t and t_2^ν, see Fig. 2-b.

B. Electron-Phonon Self-Energies

Because two degrees of freedom are confined in the CNT, an electron can only be scattered forward or backward in the axial direction, preserving or changing the sign of the band-velocity, respectively. We assume bias conditions for

which the first subband predominantly contributes to the total current and only intra-subband intra-valley transitions have to be considered.

A linear dispersion relation for acoustic phonons is assumed, $\omega_{q,\lambda} \approx \upsilon_\lambda |q|$, where υ_λ is the acoustic phonon velocity and λ is the phonon polarization. For optical phonons the energy is assumed to be independent of the phonon wave-vector $\omega_{q,\lambda} \approx \omega_{\mathrm{OP},\lambda} = \mathrm{const}$. Similarly, the matrix elements of electron-phonon interaction [19] can be approximated as $M_{q,\lambda} \approx M_\lambda^{\mathrm{AP}}|q|$ for acoustic phonons and $M_{q,\lambda} \approx M_\lambda^{\mathrm{OP}} = \mathrm{const}$ for optical phonons. The interaction of electrons with optical phonons is inelastic. Assuming that the electron-phonon interaction occurs locally [20], the self-energies can be written as

$$\Sigma_{\mathrm{inel}}^{<,\nu}(E) = \sum_\lambda D_{\mathrm{inel},\lambda} \times [(N_\lambda + 1)\, G^{<,\nu}(E + \hbar\omega_\lambda) + N_\lambda G^{<,\nu}(E - \hbar\omega_\lambda)] \quad (7)$$

$$\Sigma_{\mathrm{inel}}^{>,\nu}(E) = \sum_\lambda D_{\mathrm{inel},\lambda} \times [(N_\lambda + 1)\, G^{>,\nu}(E - \hbar\omega_\lambda) + N_\lambda G^{>,\nu}(E + \hbar\omega_\lambda)] \quad (8)$$

where N_λ is the phonon occupation number which is given by the Bose-Einstein distribution function. The electron-phonon interaction strength is given by

$$D_{\mathrm{inel},\lambda} = \frac{\hbar |M_\lambda^{\mathrm{OP}}|^2}{2 n m_{\mathrm{c}} \omega_\lambda} \quad (9)$$

where m_{c} is the mass of a carbon atom. The first term in (7) corresponds to the emission of a phonon by the de-excitation of an electron and the second term corresponds to the excitation of an electron by the absorption of a phonon. Interaction with acoustic phonons can be regarded as elastic scattering, $E \pm \hbar\omega_\lambda \approx E$, and the approximation $N_\lambda \approx N_\lambda + 1 \approx k_{\mathrm{B}} T / \hbar \upsilon_\lambda$ can be used. Based on this approximation, the self-energies for acoustic phonon interaction simplify to

$$\Sigma_{\mathrm{el}}^{\lessgtr,\nu}(E) = D_{\mathrm{el}}^\nu G^{\lessgtr,\nu}(E) \quad (10)$$

$$D_{\mathrm{el},\lambda} = \frac{k_{\mathrm{B}} T |M_\lambda^{\mathrm{AP}}|^2}{n m_{\mathrm{c}} \upsilon_\lambda} \quad (11)$$

The self-energy due to electron-phonon interaction comprises the contributions of elastic and inelastic scattering mechanisms, $\Sigma_{\mathrm{e-ph}}^\nu = \Sigma_{\mathrm{el}}^\nu + \Sigma_{\mathrm{inel}}^\nu$. The transport equations must be iterated to achieve convergence of the electron-phonon self-energies, resulting in a self-consistent Born approximation [21].

C. Self-Consistent Simulations

To solve transport equations numerically they need to be discretized in both the spatial and the energy domain. The carrier concentration at some node l of the spatial grid and the current density at the edge between the nodes l and $l+1$ are given by

$$n_l = -4i \sum_\nu \int \frac{dE}{2\pi} G_{l,l}^{<,\nu}(E) \quad (12)$$

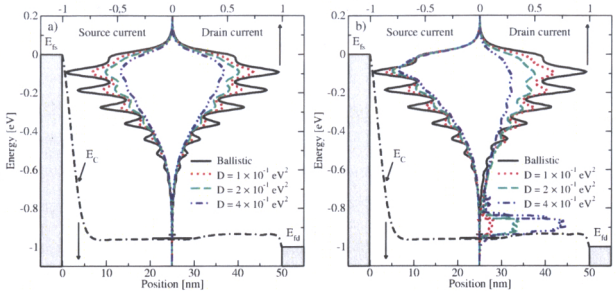

Fig. 3. The spectra of the source and drain currents. a) The effect of elastic phonon scattering and b) the effect of inelastic phonon scattering with different coupling strengths are shown. The phonon energy is $\hbar\omega = 100$ meV.

$$j_{l,l+1} = \frac{4\mathrm{q}}{\hbar} \sum_\nu \int \frac{dE}{2\pi} 2\Re e\{G_{l,l+1}^{<,\nu}(E) t_{l+1,l}^\nu\} \quad (13)$$

where the factor 4 is due to spin and band degeneracy.

For an accurate analysis it is essential to solve the coupled system of transport equations and the Poisson equation self-consistently [17]. The convergence of the self-consistent iteration is a critical issue. To achieve convergence, fine resonances at some energies in (12) have to be resolved accurately. For that purpose an adaptive method for selecting the energy grid is essential [22].

IV. Electron-Phonon Interaction in CNTs

Fig. 3 compares the current spectrum in the absence and presence of electron-phonon interaction. Elastic scattering conserves the energy of carriers, but the current decreases due to elastic back-scattering of carriers. Fig. 3-a shows that for elastic scattering the source and drain current spectra are symmetric. As the electron-phonon coupling strength increases, resonances in the current spectrum are washed out and the total current decreases due to elastic back-scattering.

In the case of inelastic scattering, carriers acquiring enough kinetic energy can emit a phonon and scatter into lower energy states [14]. Therefore, as shown in Fig. 3-b, the source and drain current spectra are not symmetric. As the coupling strength increases, more electrons are scattered into lower energy states.

Fig. 4 shows the spectra of the source and drain currents for different inelastic phonon energies. Electrons can emit a single phonon or a couple of phonons to reach lower energy states. The probability of multiple phonon emissions decreases as the number of interactions increases. Therefore, as the phonon energy increases, the occupation of electrons at lower energy states increases.

As shown in Fig. 4-b, the electron population close to the conduction band-edge considerably increases as the phonon energy increases. Therefore, as the phonon energy increases the mean velocity of electrons decreases and the carrier concentration in the channel increases. The increased charge in the channel results in an increased gate-delay time [14].

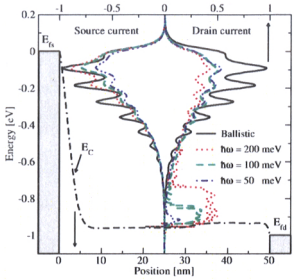

Fig. 4. The spectra of the source and drain currents. The effect of inelastic scattering with different phonon energies is shown. The electron-phonon coupling strength is $D = 2 \times 10^{-1}$ eV^2. A considerable increase of the electron population close to the conduction band-edge as the phonon energy increases can be seen.

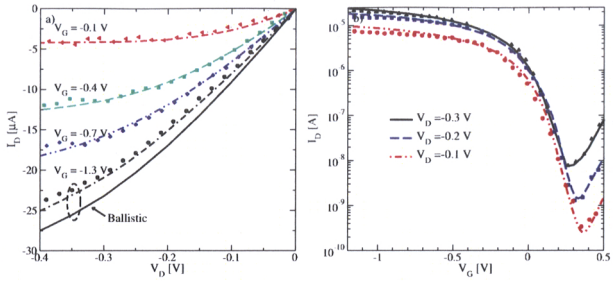

Fig. 5. Comparison of the simulation results and experimental data for the a) output and b) transfer characteristics. Lines show the simulation results and symbols show experimental data. The result for $V_G = -1.3$ V is compared with the ballistic limit. Experimental data have been adopted from [25].

V. Discussion

In general the electron-phonon interaction parameters depend on the diameter and the chirality of a CNT [19]. CNTs with a diameter $d_{\mathrm{CNT}} > 2$ nm have a band gap $E_{\mathrm{G}} < 0.4$ eV, which renders them unsuitable as channel for transistors. Since the fabrication of devices with a diameter $d_{\mathrm{CNT}} < 1$ nm is very difficult, we limit our study to zigzag CNTs with diameters in the range of $d_{\mathrm{CNT}} = 1 - 2$ nm.

Scattering with acoustic phonons is treated as an elastic process. The electron-phonon coupling is also weak for acoustic phonons ($D_{\mathrm{AP}} < 10^{-3}$ eV^2), which implies that elastic back-scattering of carriers is weak. Inelastic scattering is induced by optical (OP), radial breathing mode (RBM), and K-point phonons [23]. Considering the class of CNTs discussed above, energies of these phonons are $\hbar\omega_{\mathrm{OP}} \approx 200$ meV, $\hbar\omega_{\mathrm{RBM}} \approx 25$ meV, and $\hbar\omega_{\mathrm{K_1}} \approx 160$ meV and $\hbar\omega_{\mathrm{K_2}} \approx 180$ meV [23, 24]. The corresponding coupling coefficients are $D_{\mathrm{OP}} \approx 40 \times 10^{-3}$ eV^2, $D_{\mathrm{RBM}} \approx 10^{-3}$ eV^2, and $D_{\mathrm{K_1}} \approx 10^{-4}$ eV^2, and $D_{\mathrm{K_2}} \approx 10^{-3}$ eV^2 [24].

As discussed in Section IV, high energy phonons such as OP and K-point phonons reduce the on-current only weakly, but they can increase the gate-delay time considerably due to charge pileup in the channel [14]. Low energy phonons such as the RBM phonon can reduce the on-current more effectively, but these have a weaker effect on the gate-delay time. However, due to strong coupling, scattering processes are mostly due to electron-phonon interaction with high energy phonons. Therefore, at room temperature the on-current of short CNT-FETs can be close to the ballistic limit [25] (see Fig. 5), whereas the gate-delay time can be significantly below that limit [26].

The intrinsic (without parasitic capacitances) gate-delay time for the ballistic case can be fitted as $\tau \approx 1.7$ ps/μm, or equivalently $f_T \approx 100$ GHz/μm [27]. The highest reported intrinsic cutoff frequency for a device with a length of 300 nm is $f_T \approx 30$ GHz [28], which is far below the ballistic limit. Inelastic electron-phonon interaction with high energy phonons has to be considered to explain the results.

VI. Conclusion

The coupled system of transport and Poisson equations was solved self-consistently. A tight-binding Hamiltonian is used to describe transport phenomena in CNT-FETs. Employing the described model, both, the static and dynamic response of CNT-FETs was investigated. The effect of electron-phonon interaction on the device characteristics is discussed in detail. In agreement with experimental data, our results indicate that at room temperature electron phonon interaction affects the steady-state current of CNT-FETs only weakly, whereas the switching response can be significantly affected.

Acknowledgment

This work, as part of the European Science Foundation EUROCORES Programme FoNE, was supported by funds from FWF (Contract I79-N16), CNR, EPSRC and the EC Sixth Framework Programme, under Contract No. ERAS-CT-2003-980409.

References

[1] R. Martel *et al.*, Appl. Phys. Lett. **73**, 2447 (1998).
[2] W. Hoenlein *et al.*, IEEE Trans. Comp. Packag. Technol. **27**, 629 (2004).
[3] J. Appenzeller, Proc. IEEE **96**, 201 (2008).
[4] P. Avouris *et al.*, Nature Nanotechnology **2**, 605 (2007).
[5] A. Javey *et al.*, Nature (London) **424**, 654 (2003).
[6] R. V. Seidel *et al.*, Nano Lett. **5**, 147 (2005).
[7] J.-Y. Park, Nanotechnology **18**, 095202 (2007).
[8] M. Freitag *et al.*, Phys. Rev. Lett. **93**, 076803 (2004).
[9] M. Freitag *et al.*, Nano Lett. **3**, 1067 (2003).
[10] A. Svizhenko *et al.*, J. Appl. Phys. **91**, 2343 (2002).
[11] R. Venugopal *et al.*, J. Appl. Phys. **92**, 3730 (2002).
[12] J. Guo, J. Appl. Phys. **98**, 063519 (2005).
[13] A. Svizhenko *et al.*, Phys. Rev. B **72**, 085430 (2005).
[14] M. Pourfath *et al.*, Nanotechnology **18**, 424036 (2007).
[15] W. Tian *et al.*, J. Chem. Phys **109**, 2874 (1998).
[16] Y. Xue *et al.*, Appl. Phys. Lett. **83**, 2429 (2003).
[17] A. W. Ghosh *et al.*, Nano Lett. **4**, 565 (2004).
[18] S. Datta, Superlattices Microstruct. **28**, 253 (2000).
[19] V. N. Popov *et al.*, Phys. Rev. B **74**, 075415 (2006).
[20] R. Lake *et al.*, Phys. Rev. B **45**, 6670 (1992).
[21] R. Lake *et al.*, J. Appl. Phys. **81**, 7845 (1997).
[22] M. Pourfath *et al.*, J. Comp. Electronics **5**, 155 (2006).
[23] J. Park *et al.*, Nano Lett. **4**, 517 (2004).
[24] S. O. Koswatta *et al.*, Appl. Phys. Lett. **89**, 023125 (2006).
[25] A. Javey *et al.*, Nano Lett. **4**, 1319 (2004).
[26] X. Huo *et al.*, in *Intl. Electron Device Meet. Tech. Dig.* 691 (2004)
[27] Y. Yoon *et al.*, IEEE Trans. Electron Devices **53**, 2467 (2006).
[28] A. L. Louarn *et al.*, Appl. Phys. Lett. **90**, 233108 (2007).